

Highly Selective Cross-Etherification of 5-Hydroxymethylfurfural with Ethanol

Supporting Information

Meredith C. Allen,^{1,2,†} Alexander J. Hoffman,^{3, †} Tsung-wei Liu,^{3,§} Matthew S. Webber,¹ David Hibbitts,^{3} Thomas J. Schwartz^{1,2,4*}*

1. Department of Chemical and Biomedical Engineering, University of Maine, Orono, ME 04469
2. Forest Bioproducts Research Institute, University of Maine, Orono, ME 04469
3. Department of Chemical Engineering, University of Florida, Gainesville, FL 32612
4. Frontier Institute for Research in Sensor Technology, University of Maine, Orono, ME 04469

†These authors contributed equally to this work.

§Current address: Dept. of Chemical and Biological Engineering, Colorado School of Mines, Golden, CO 80401

*To whom correspondence should be addressed: hibbitts@che.ufl.edu & thomas.schwartz@maine.edu

Table of Contents

S.1. Effect of acid sites types and catalyst geometry on EMF production	S3
S.2. Estimation of enthalpies, free energies, and entropy for DFT calculations	S4
S.3. Tabulation of activity coefficients, activities, and equivalent pressures	S5
S.4. DFT-calculated structures of transition states and surface intermediates	S6
S.5. Gas-phase carbocation exchange energetics	S10
S.6. DFT-predicted rates of competing etherification pathways	S11
S.7. Effect of altered permittivity from VASPsol on predicted DFT rates	S12
S.8. References.....	S13

List of Figures and Tables

Table S1	S3
Table S2	S5
Table S3	S10
Figure S1	S3
Figure S2	S3
Figure S3	S6
Figure S4.....	S7
Figure S5.....	S8
Figure S6.....	S9
Figure S7.....	S10
Figure S8.....	S10
Figure S9.....	S11
Figure S10.....	S12

S.1. Effect of acid site types and catalyst geometry on EMF production

Table S1. Tabulation of Brønsted and Lewis acid sites obtained by FTIR spectroscopy of adsorbed pyridine.

Catalyst	Area of Brønsted	Area of Lewis	Area Physisorbed	Absorbance Brønsted/Lewis	Concentration Brønsted/Lewis
Mordenite	2.58	0.03	0.11	98.98	74.46
Y-Zeolite	5.59	2.87	0.13	1.95	1.47
ZSM-5	7.37	0.33	0.92	22.17	16.68
B-25	7.44	2.68	1.41	2.77	2.09
B-38	5.01	1.71	1.65	2.93	2.20
B-300	2.15	0.18	0.45	11.89	8.94

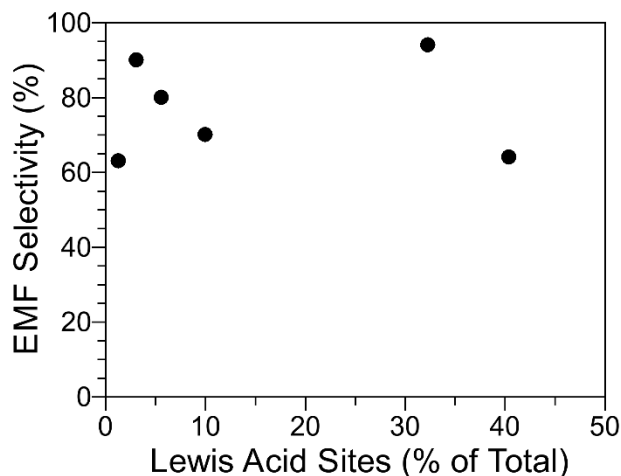


Figure S1. Influence of Lewis acidity on the selectivity to EMF.

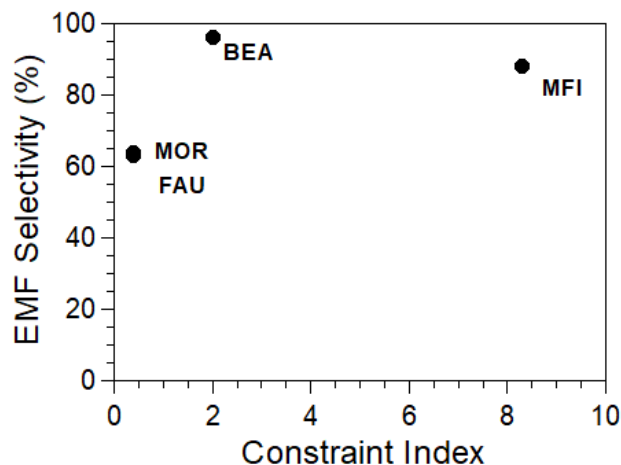


Figure S2. Influence of the constraint index on the selectivity to EMF, showing that the BEA geometry is optimal for EMF production. Note the points for MOR and FAU overlap (see Table 1 in the main text). Values for the constraint index are from Jae *et al.* [1] and Frillette *et al.* [2].

S.2. Estimation of enthalpies, free energies, and entropy for DFT calculations

Enthalpies and free energies were calculated by summing DFT-calculated electronic energy, ZPVE, and vibrational, rotational, and translational enthalpies (H_{vib} , H_{rot} , H_{trans}) or free energies (G_{vib} , G_{rot} , G_{trans}) based on the fixed displacement methods described in the main text. Adsorbate and transition state motions in zeolite frameworks were considered vibrations—that is, rotation and translation H and G are zero for species within the framework. All framework Si and O atoms were frozen in place during frequency calculations, except for O atoms attached to framework Al atoms. Vibrational energies, enthalpies, and free energies were calculated from statistical mechanics:^[1]

$$ZPVE = \sum_i \left(\frac{1}{2} h\nu_i \right) \quad (S1)$$

$$H_{vib} = \sum_i \left(\frac{h\nu_i \exp\left(-\frac{h\nu_i}{kT}\right)}{1 - \exp\left(-\frac{h\nu_i}{kT}\right)} \right) \quad (S2)$$

$$H_{vib} = \sum_i \left(-kT \ln \left(\frac{1}{1 - \exp\left(-\frac{h\nu_i}{kT}\right)} \right) \right) \quad (S3)$$

Translational and rotational H and G are calculated for all gas-phase species from first principles:

$$H_{trans} = \frac{5}{2} k_B T \quad (S4)$$

$$H_{rot,linear} = k_B T \quad (S5)$$

$$H_{rot,nonlinear} = \frac{3}{2} k_B T \quad (S6)$$

$$G_{trans} = -k_B T \ln \left(\left(\frac{2\pi M k_B T}{h^2} \right)^{\frac{3}{2}} V \right) \quad (S7)$$

$$G_{rot} = -k_B T \ln \left(\frac{\pi^2}{\sigma} \left(\frac{T^3}{\theta_x \theta_y \theta_z} \right)^{\frac{1}{2}} \right) \quad (S8)$$

$$\theta_i = \frac{h^2}{8\pi^2 k_B I_i} \quad (S9)$$

where I_i is the moment of inertial about each axis and σ is the symmetry number. Entropies (S) are calculated from H and G at 433 K:

$$S = \frac{H-G}{T} \quad (S10)$$

S.3. Tabulation of activity coefficients, activities, and equivalent pressures

Table S2. Conversion to partial pressures using UNIFAC to derive activity coefficients (γ) and subsequent partial pressures.

Concentrations mol L ⁻¹		Activity Coefficients (γ)			Partial Pressures mbar		
HMF	C ₂ H ₅ OH	HMF	C ₂ H ₅ OH	H ₂ O	HMF	C ₂ H ₅ OH	H ₂ O
0.016	12.900	9.50	2.03	3.41	0.06	243.05	737.09
0.030	12.900	9.47	2.03	3.40	0.11	242.30	736.47
0.093	12.900	9.37	2.06	3.35	0.33	238.92	733.67
0.093	12.900	9.37	2.06	3.35	0.33	238.89	733.65
0.108	12.900	9.35	2.07	3.34	0.38	238.12	733.02
0.123	12.900	9.32	2.07	3.33	0.43	237.32	732.37
0.125	12.900	9.32	2.07	3.33	0.44	237.23	732.30
0.125	12.900	9.32	2.07	3.33	0.44	237.21	732.27
0.080	0.324	5.90	3.14	1.73	0.06	3.11	543.61
0.080	0.375	5.91	3.14	1.73	0.06	3.61	543.96
0.080	0.433	5.92	3.13	1.73	0.06	4.17	544.35
0.080	0.601	5.94	3.12	1.74	0.06	5.83	545.51
0.080	12.662	9.30	2.09	3.25	0.28	230.62	727.31
0.080	12.662	9.30	2.09	3.25	0.28	230.64	727.32
0.080	12.695	9.31	2.08	3.26	0.28	231.84	728.26

S.4. DFT-calculated structures of transition states and surface intermediates

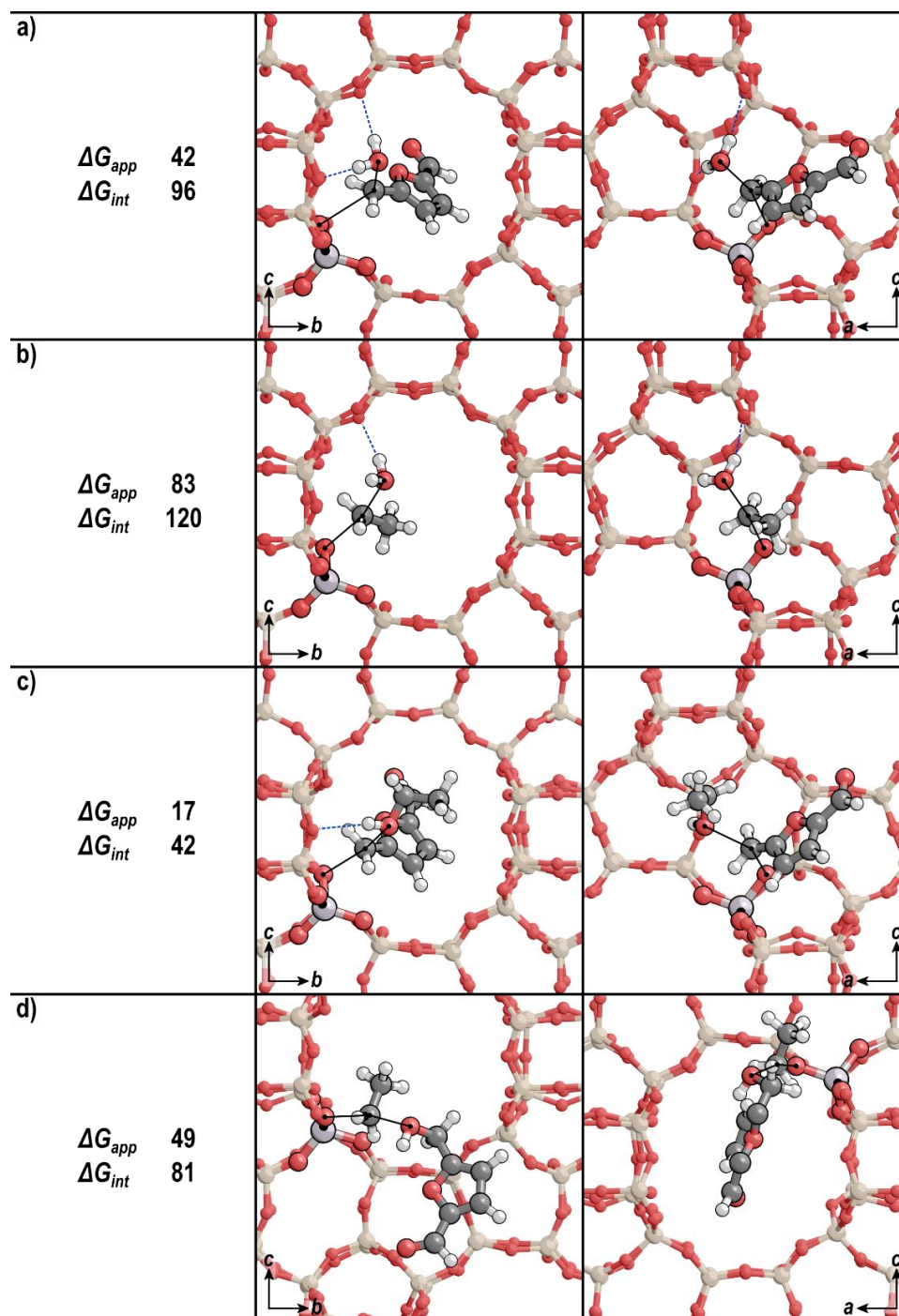


Figure S3. The best transition states found for (a) the first step of the sequential route via HMF dehydration, (b) the first step of the sequential route via ethanol dehydration, (c) the second step of the sequential route via a methylfurfural cation, and (d) the second step of the sequential route via an ethyl cation. Incipient and breaking bonds are indicated with solid black lines and H-bonds are indicated with dashed blue lines. Apparent free energy barriers (ΔG_{app}) relative to a bare proton and intrinsic free energy barriers (ΔG_{int}) are shown in kJ mol^{-1} .

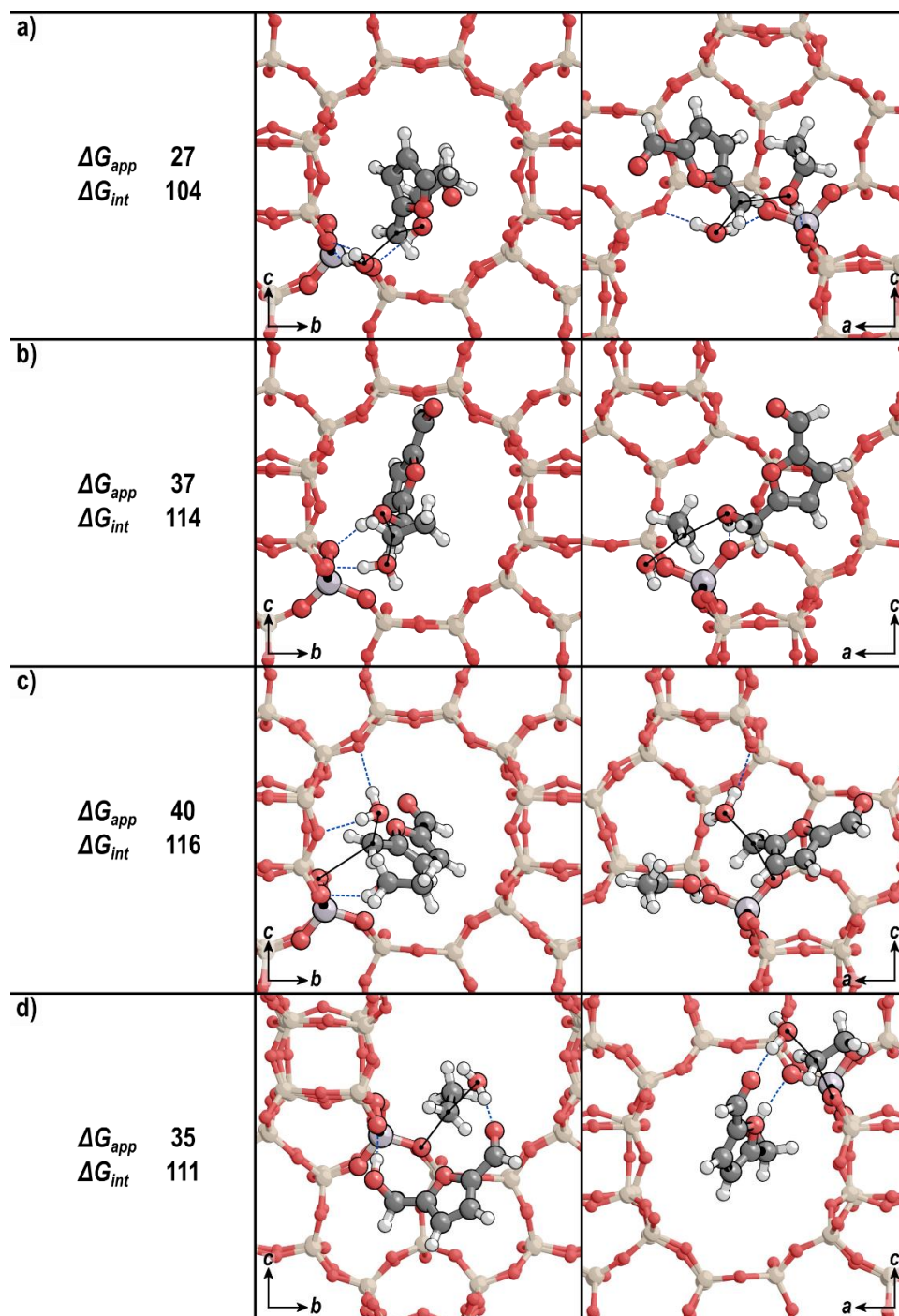


Figure S4. The best transition states found for (a) the concerted route via HMF dehydration, (b) the concerted route via ethanol dehydration, (c) the first step of the sequential route via HMF dehydration with spectating C_2H_5OH , (d) the first step of the sequential route via ethanol dehydration with spectating HMF. Incipient and breaking bonds are indicated with solid black lines and H-bonds are indicated with dashed blue lines. Apparent free energy barriers (ΔG_{app}) relative to a bare proton and intrinsic free energy barriers (ΔG_{int}) are shown in kJ mol^{-1} .

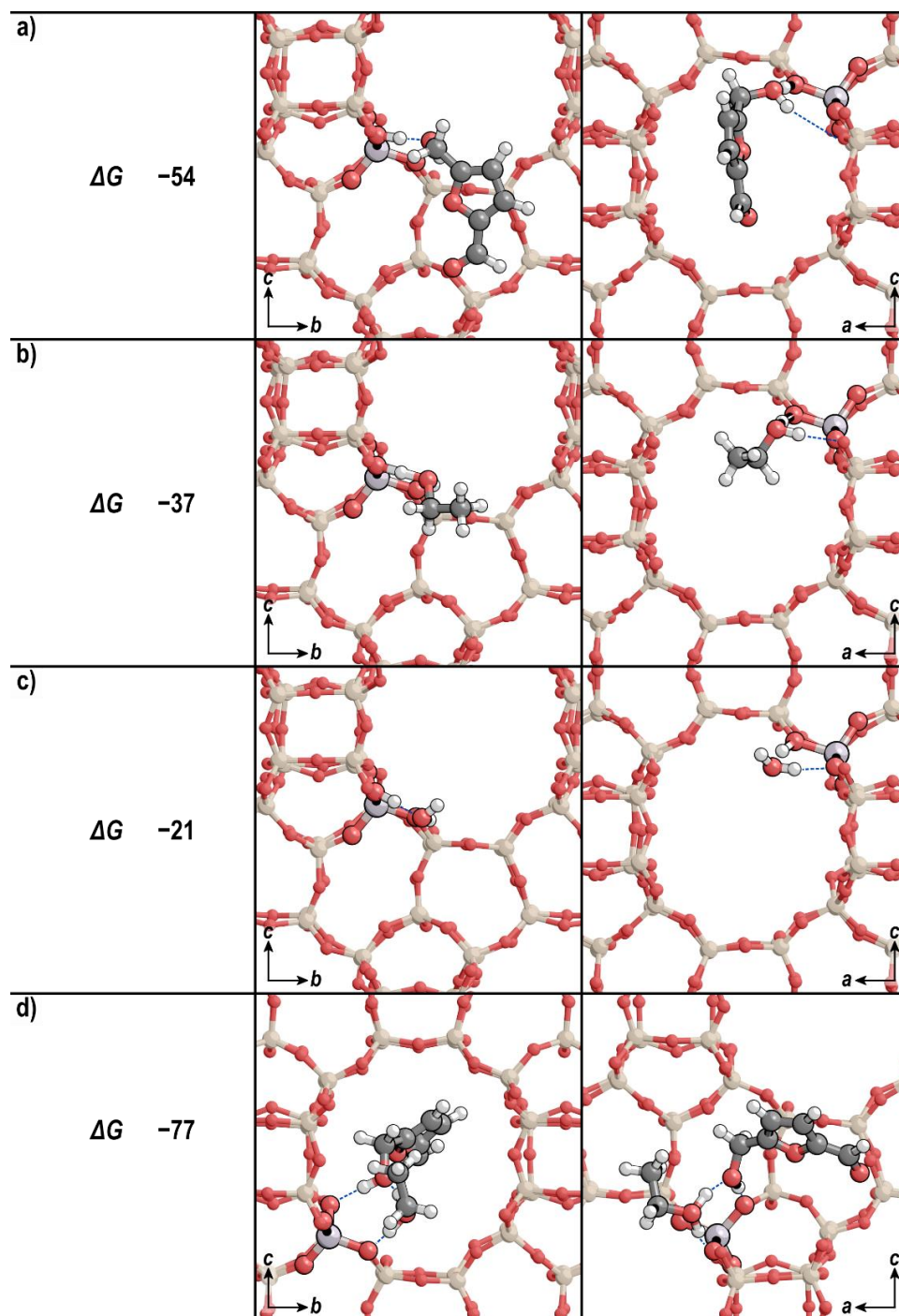


Figure S5. Structures of abundant surface intermediates: (a) an HMF monomer, (b) a C_2H_5OH monomer, (c) a water monomer, and (d) a C_2H_5OH -HMF dimer complex. H-bonds are indicated with dashed blue lines. Free energy values (ΔG) are shown relative to a bare proton in kJ mol^{-1} .

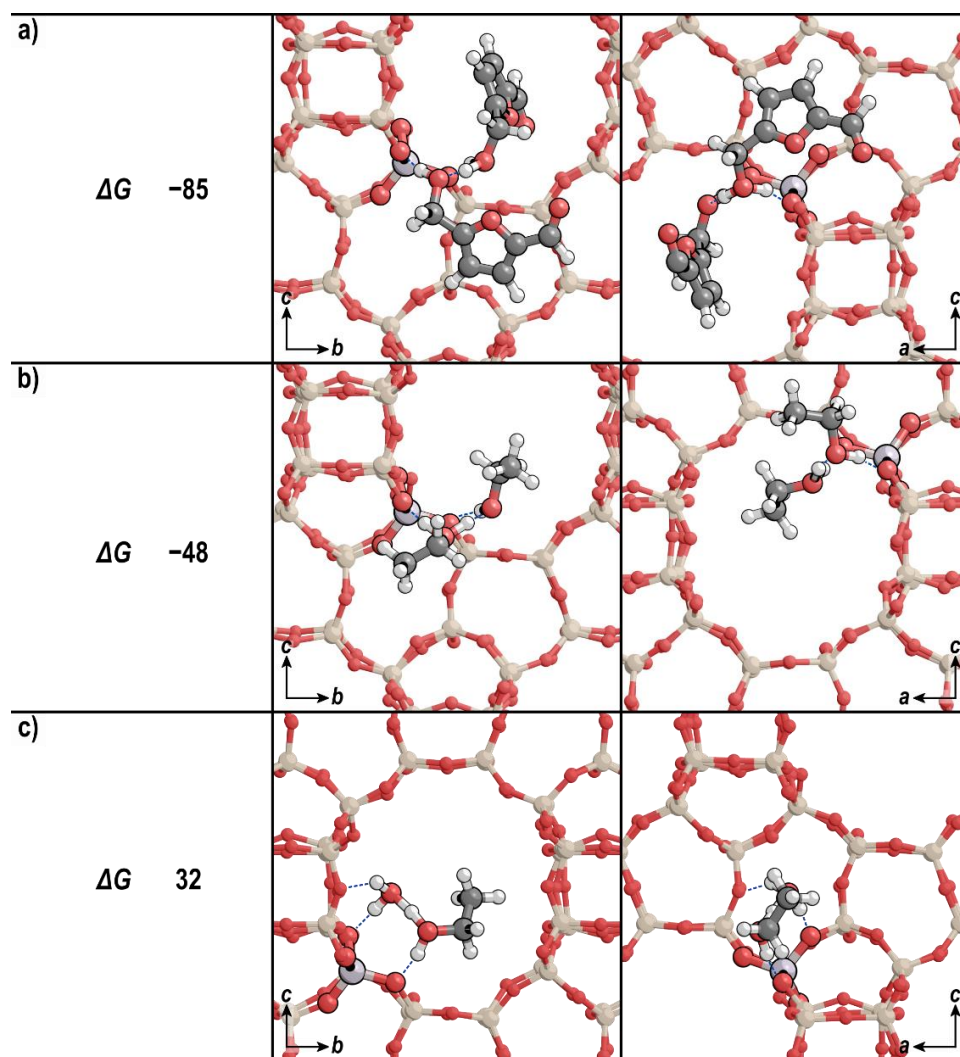


Figure S6. Structures of abundant surface intermediates: (a) an HMF-HMF dimer complex, (b) a $\text{C}_2\text{H}_5\text{OH}-\text{C}_2\text{H}_5\text{OH}$ dimer complex, and (c) a $\text{C}_2\text{H}_5\text{OH}-\text{H}_2\text{O}$ dimer complex. H-bonds are indicated with dashed blue lines. Free energy values (ΔG) are shown relative to a bare proton in kJ mol^{-1} .

S.5. Gas-phase carbocation exchange energetics and methylfurfural carbocation resonance structures

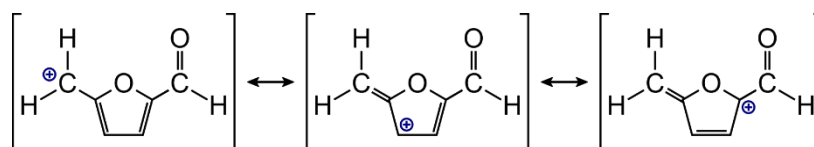


Figure S7. Possible resonance structures for the methylfurfural (MF^+) carbocation.

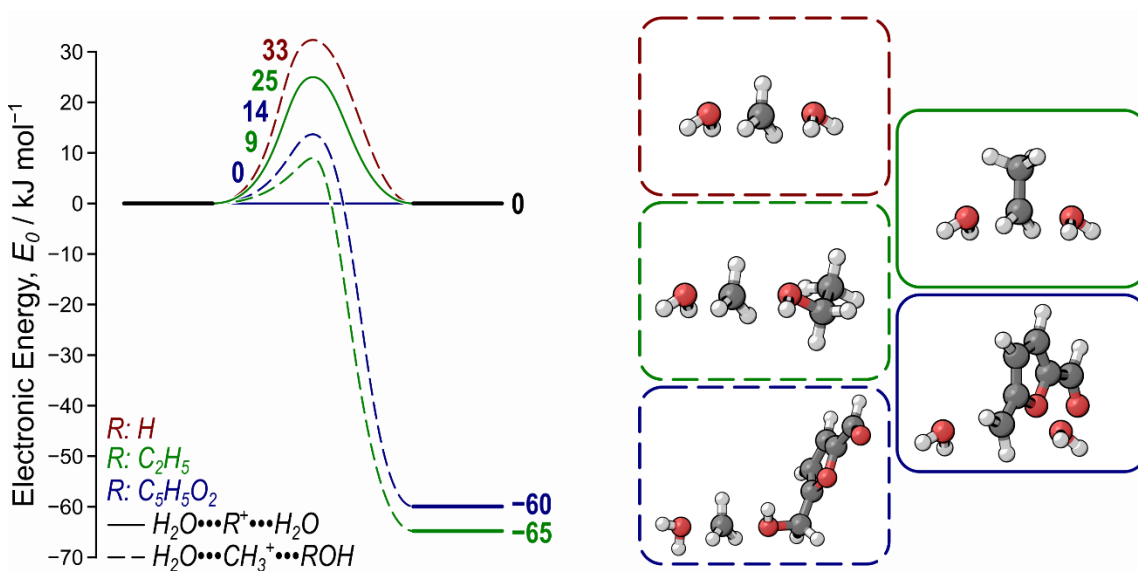


Figure S8. Reaction coordinate diagrams for alkyl transfer reactions in the gas phase. Solid lines indicate ethyl (C_2H_5^+ , green) and methylfurfural ($\text{C}_5\text{H}_5\text{O}_2^+$, blue) transfer between two H_2O molecules. Dashed lines indicate the energy required to methylate a water molecule (red), ethanol (green), and HMF (blue), with their associated transition states to the right.

Table S3. Barriers for alkyl group transfers between two water molecules from alcohols with which etherification reactions with HMF were examined.

Alcohol	Barrier kJ mol^{-1}
5-Hydroxymethylfurfural	0
Ethanol	25
<i>n</i> -Butanol	36
Cyclohexanol	49
Phenol	82

S.6. DFT-predicted rates of competing etherification pathways

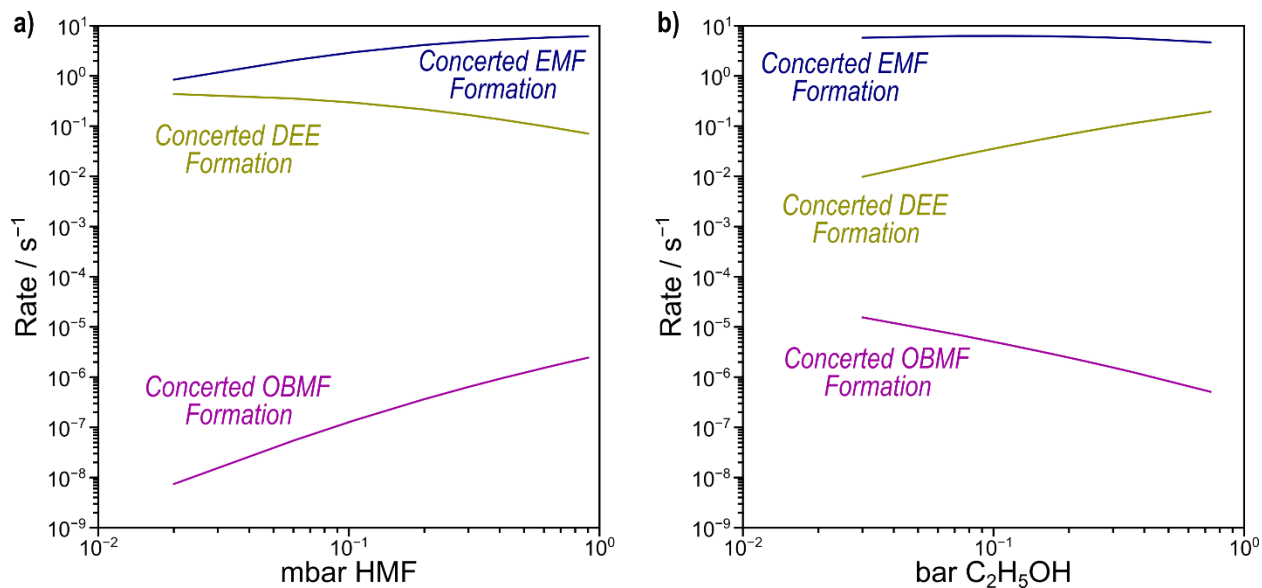


Figure S9. Predicted rates of concerted EMF formation via HMF dehydration (blue), concerted diethyl ether (DEE) formation (yellow), and concerted 5,5'-oxy(bismethylene)-2-furaldehyde (OBMF) formation (magenta) with changing (a) HMF and (b) C₂H₅OH pressure.

S.7. Effect of altered permittivity from VASPsol on predicted DFT rates

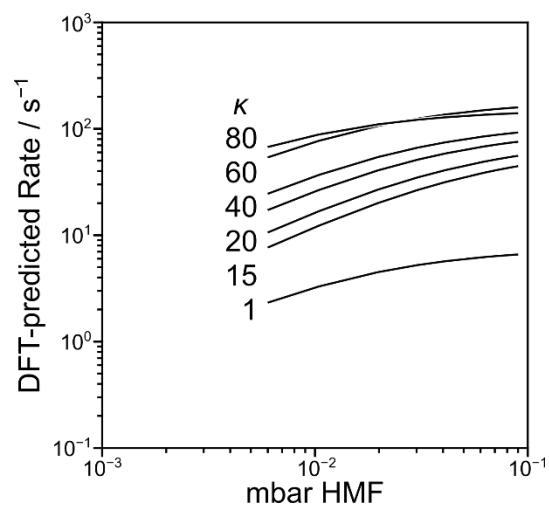


Figure S10. Predicted rates of EMF formation from DFT with VASPsol-adjusted relative permittivities at 1 to 80.

S.8. References

[1] Jae, J.; Tompsett, G. A.; Foster, A. J.; Hammond, K. D.; Auerbach, S. M.; Lobo, R. F.; Huber, G. W., Investigation into the shape selectivity of zeolite catalysts for biomass conversion. *Journal of Catalysis* **2011**, 279, 257-268.

[2] Frillette, V. J.; Haag, W. O.; Lago, R. M., Catalysis by Crystalline Aluminosilicates: Characterization of Intermediate Pore-Size Zeolites by the “Constraint Index”. *Journal of Catalysis* **1981**, 67, 218-222.